Vibrational couplings between protein and cofactor in bacterial phytochrome Agp1 revealed by 2D-IR spectroscopy

David Buhrke[a,1] , Norbert Michael[b] , and Peter Hamm[a]

Phytochromes are ubiquitous photoreceptor proteins that undergo a significant refolding of secondary structure in response to initial photoisomerization of the chromophoric group. This process is important for the signal transduction through the protein and thus its regulatory function in different organisms. Here, we employ two-dimensional infrared absorption (2D-IR) spectroscopy, an ultrafast spectroscopic technique that is sensitive to vibrational couplings, to study the photoreaction of bacterial phytochrome Agp1. By calculating difference spectra with respect to the photoactivation, we are able to isolate sharp difference cross-peaks that report on local changes in vibrational couplings between different sites of the chromophore and the protein. These results indicate inter alia that a dipole coupling between the chromophore and the so-called tongue region plays a role in stabilizing the protein in the light-activated state.

biophysics | phytochrome | 2D-IR | protein folding | spectroscopy

Phytochromes are photoreceptive proteins with variable domain architecture (1) that many different organisms, such as plants (2), fungi (3), cyanobacteria (4), and bacteria (5) use to sense light. All phytochromes bind open-chain tetrapyrrole chromophores, like biliverdin Xα (BV) (mainly in bacterial variants) (6), and convert between two "parent" states with distinct absorption spectra. Bacterial phytochromes (Bphs) are of specific interest within this diverse class of proteins, because they can be easily expressed, purified, modified, and used in biotechnological applications such as optogenetics or fluorescence microscopy (7, 8).

Bphs act as light-driven enzymes in bacterial two-component signaling, e.g., light-activated histidine kinases (9), phosphatases (10), or cyclases (11). They photoswitch between a red-absorbing (Pr) and a far-red absorbing (Pfr) state, thereby regulating the according C-terminal catalytic domain, which is typically located several nanometers away from the chromophore. Due to this large distance, the light regulation of enzymatic activity involves an intricate mechanism: an initial light-triggered Z/E isomerization of BV causes refolding of a nearby secondary structure element (the "tongue" region, Fig. 1), resulting in functional tertiary structure rearrangements of the catalytic domain (8). The light-induced transition of the tongue is a rather dramatic structural change as it comprises the repositioning of all involved amino acids and the breaking and formation of tens of hydrogen bonds. Due to its magnitude, it is often viewed as the critical step in intramolecular signal amplification (12).

Over the last decades, many analytic techniques such as X-ray crystallography (13, 14), NMR spectroscopy (15), cryo-electron microscopy (16), time-resolved X-ray solution scattering (12, 17), and molecular dynamics simulations (18) have been used to probe the molecular details of this complex reaction cascade. On top of that, vibrational spectroscopies (resonance Raman [RR] and infrared absorption [IR]) had a strong contribution to the current understanding of the phytochrome photoreactions due to their high intrinsic time resolution, sensitivity to subtle changes in molecular geometries, and applicability to solution samples at physiological temperatures (19–23). IR difference spectroscopy was mainly employed in the amide I region, where the frequency changes of C = C and C = O stretching modes of the chromophore (24) can be followed in the same spectral window as the backbone amide I modes, which report, e.g., on the tongue transition between β-hairpin and α-helical states (19, 25, 26).

Since the different contributions in this information-rich region overlap strongly and partly cancel each other, clear assignments and quantitative measurements are unfortunately seriously aggravated in IR difference spectroscopy. Here, we attempt to partially overcome this problem by spreading the spectrum out into two dimensions using two-dimensional infrared absorption (2D-IR) difference spectroscopy. Two-dimensional IR is an advanced femtosecond IR-pump/IR-probe technique with a frequency-resolved pump axis that provides additional observables such as 2D lineshape and cross-peaks that are inaccessible by linear spectroscopy (27, 28). Furthermore, 2D-IR spectroscopy is,

Significance

Two-dimensional infrared absorption (2D-IR) spectroscopy is severely limited in its application to larger proteins due to broad and overlapping signals in the amide I region. Here, we overcome this limitation and isolate couplings between pairwise two single-molecular groups in the biotechnologically relevant phytochrome Agp1 (510 aa) by calculating light-induced difference spectra. In phytochromes, the photoactivation of a cofactor with a relatively small structural change triggers a large-scale refolding of big parts of the protein, but the mechanism of that interaction is not understood. We observe cross-peaks in the 2D-IR spectra that are directly related to the changing dipole coupling between the cofactor and the part of the protein that refolds, suggesting that both sites stabilize each other mutually.

Author affiliations: [a]Department of Chemistry, University of Zürich, CH-8057 Zürich, Switzerland; and [b]Department of Chemistry, Technical University Berlin, 10623 Berlin, Germany

[1]To whom correspondence may be addressed. Email: david.buhrke@chem.uzh.ch.
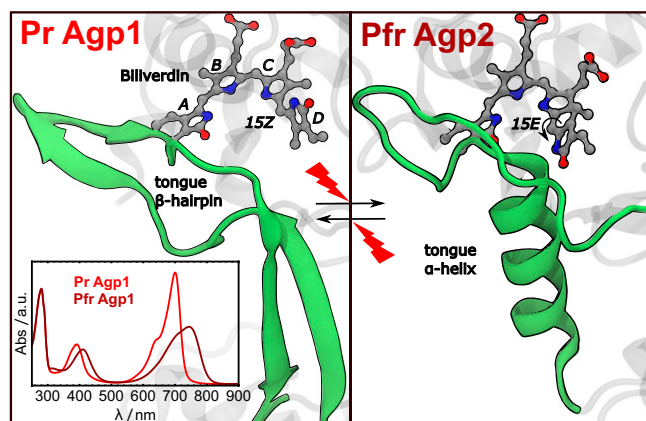
Fig. 1. The red/far-red photochemistry of canonical Bphs. (*Left*) Detailed view of the crystal structure of Agp1 in the Pr state (Protein Data Bank [PDB] code 5HSQ), with the BV chromophore in the *15Z* configuration and the tongue region as a hairpin fold. (*Right*) The crystal structure of the Pfr-stabilized phytochrome Agp2 can be used as a model for Agp1 in the Pfr state (PDB code 6G1Y). In Pfr, BV adopts the *15E* configuration and the tongue forms a helix. *Inset* shows vis absorption spectra of Agp1 in Pr and Pfr.

in contrast to linear techniques, sensitive to vibrational couplings. Due to these advantages, 2D-IR offers a direct way to study the connectivity between different functional groups in phytochromes via cross-peaks as a function of the photocycle and thus reveals insights into the molecular mechanism of the signal transduction in solution with high time resolution.

We selected the canonical bacterial phytochrome Agp1 from *Agrobacterium fabrum* (9, 29) as a model system, because this specific Bph has been studied extensively with X-ray crystallography and linear vibrational spectroscopy, providing a solid reference for the 2D measurements (20, 23, 30, 31). Since no crystal structure of Agp1 in the Pfr state is available, the crystal structure of the Pfr-stabilized phytochrome Agp2 is used as a model for the Pfr state of Agp1 throughout this article (32). Within that frame, we find that the 2D-IR measurements provide a large amount of interesting information such as changes in lineshapes and cross-peaks that allow us to dissect the IR spectrum and propose a model for the kinetic stabilization of the Pfr state.

Results

2D-IR Spectroscopy in the Pfr and Pr States. To set the stage, absolute 2D-IR spectra of Agp1 were measured in the Pr and Pfr

states by illuminating the sample inside the spectrometer. While the Pr state can be populated with this procedure essentially pure, the Pfr spectrum can contain a residual Pr contribution (compare ultraviolet-visible [UV-vis] spectra in Fig. 1). We estimated it to be <20% by performing an iterative subtraction procedure on the vis absorption spectra $Pfr_{pure} = Pfr_{exp} - s \cdot Pr_{exp}$, varying s until negative bands appear as a clear sign of oversubstraction. In contrast to most other 2D-IR studies in the amide I region, the data presented here were taken in H_2O buffer solution (not D_2O). This was possible due to the very high solubility of the protein and resulting high concentration of the sample (ca. 10 mM) and further demonstrates that the sensitivity of 2D-IR has advanced over the last years to the point where it is feasible now to perform experiments on protein samples in H_2O. The choice to stay with H_2O ensures that in a large and complex protein like Agp1 all buried protic residues are protonated instead of producing a mixed protonation/deuteration pattern due to a partial inaccessibility for D_2O exchange, alleviating the assignment of vibrational bands.

In the absolute 2D-IR spectra of Agp1, four local maxima are detected on the main diagonal between 1,600 and 1,730 cm^{-1} (Fig. 2, roman numerals). Peaks I to III can be observed in 2D-IR spectra of most proteins and assigned to the dominant amide I modes of different secondary structure elements of the entire protein. Specifically, peak I (ca. 1,630 cm^{-1}) corresponds to the so-called β-sheet a– vibration, II (1,660 cm^{-1}) to α-helices, and III (1,685 cm^{-1}) to the β-sheet a+ mode. This assignment is based on reference spectra from pure β-sheet proteins like concanavalin A or α-helical proteins like myoglobin, which display these bands (27, 33). Furthermore, the β-sheet a– and a+ vibrations are coupled, giving rise to cross-peaks I/III that can be observed in β-sheet proteins in the form of a "Z" shape (Fig. 2, dotted line). In the case of Agp1, the dominant diagonal α-helix signal overlaps strongly with these cross-peaks, leading to a complex shape similar to that of other proteins with mixed secondary structure like ubiquitin (27). Furthermore, a water background from the HOH bending mode (34) is overlapping at with the amide I signals at 1,660 cm^{-1}, as evidenced by a more homogeneous lineshape of this band. Since the 2D-IR response scales quadratically with the extinction coefficient ε, the signal of the amide I band, whose extinction coefficient is larger, is enhanced relative to that of the water background. Consequently, the signal sizes of both are in the same order of magnitude, despite the much higher concentration of water.

Diagonal peak IV is found outside the amide I region and is assigned to the C = O stretching mode of the BV ring D carbonyl
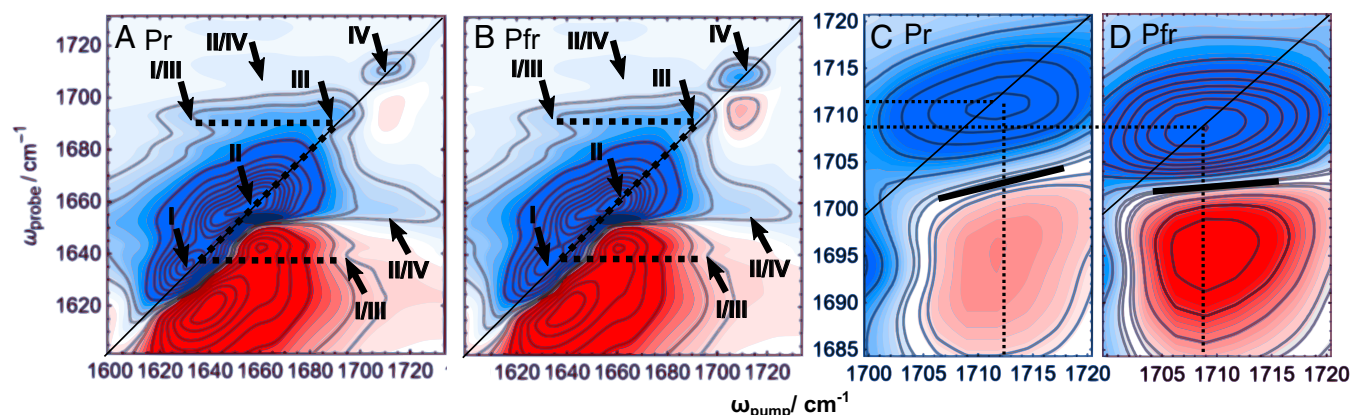

Fig. 2. The 2D-IR spectroscopy of Agp1 in the amide I region. (*A*) The 2D-IR spectrum in the Pr state. (*B*) The 2D-IR spectrum in the Pfr state. Diagonal and off-diagonal signals marked with roman numerals are discussed in detail in the main text. (*C* and *D*) Detailed view of the CO$_D$ region in the absolute Pfr and Pr spectra, with nodal line slope indicated as thick black line.

(see also Fig. 1 for nomenclature, CO_D at 1,711 cm^{-1} in Pr), in agreement with the literature, while CO_A is expected at higher frequencies (23, 24, 31). Since peak IV does not overlap with other bands, the absolute 2D lineshape can be analyzed directly in both photostates (Fig. 2 *C* and *D*). CO_D thus acts as a local vibrational probe inside the protein environment and reports on the changes of its immediate surroundings, such as hydrogen bond dynamics (35). First, CO_D is downshifted in Pfr by about 2 cm^{-1} in good agreement with previously published linear IR data (36, 37). Additionally, this mode is significantly weaker in Pr compared to Pfr. The round lineshape and nearly horizontal nodal line (thick black line in Fig. 2 *C* and *D*) in Pfr indicate that this functional group senses an ensemble of slightly different microenvironments that interchange at a rate equal to or faster than the t2 delay of 200 fs (homogeneous broadening). In contrast, the steeper nodal line and weaker peak signal in Pr indicate that CO_D is found in a more heterogeneous environment with longer interchange dynamics >200 fs. However, the actual downshift and the changes in intensity and nodal line slope might be even stronger than we report here due to a residual Pr contribution in our spectra.

Furthermore, the 2D-IR spectra reveal broad cross-peaks between CO_D and the amide I region (labeled II/IV in Fig. 2*B*), indicating vibrational coupling between CO_D and amide I in both states. Although these broad cross-peaks in the absolute spectra cannot be assigned to specific interactions with secondary structure elements, they are direct markers for protein–chromophore interactions. The subtle differences between Pr and Pfr in the amide I region are hard to analyze in the absolute spectra due to the overwhelming static amide I signal and water background. To enhance the spectral changes and simultaneously subtract out the background and the residual Pr contributions to the Pfr spectrum, the Pfr-minus-Pr difference 2D-IR spectrum was calculated.

Difference 2D-IR Spectroscopy. Fig. 3 shows the difference 2D-IR spectrum compared with the linear IR difference spectrum (Fig. 3, *Top*) and the resonance Raman (RR) spectra of Pfr and Pr (Fig. 3, *Middle*). The difference spectrum was obtained by subtracting the Pr spectrum from Pfr in a 1:1 ratio without any scaling or the like. The linear data were taken from a previous publication (37). The RR spectra allow for an assignment of vibrational modes that originate from BV, while the linear IR difference spectra selectively probe changes in vibrational frequencies between the Pfr and Pr states for both BV and protein. The dominant features on the diagonal coincide with both linear data as follows:

I) A large signal with negative sign at 1,635 cm^{-1} is mainly attributed to the loss of β-sheet a– mode due to the refolding of the tongue region, which corresponds to the largest signal in the Fourier-transform infrared (FTIR) difference spectrum.

II) A large positive signal is detected at 1,660 cm^{-1} due to folding of the tongue region into an α-helix in Pfr.

III) The β-sheet a+ mode is weak and consequently the difference upon refolding of the tongue is small. No clear difference signal is visible for this mode in either of the spectra, which is possibly also obscured by neighboring signals.

IV) The change of the CO_D lineshape upon photoconversion produces a difference pattern that closely resembles the absolute Pfr lineshape, with a small negative Pr contribution at higher frequencies. Since the CO_D is part of the conjugated system, this mode is also weakly detected in the RR spectra.

The assignment of the dominant FTIR signals that correspond to the diagonal difference bands is based on a large body of literature

(23, 25, 26, 37, 38). In these studies, it was shown that signals from other, less-defined, structural changes overlap with these signals that are typically smaller by a factor of 2 to 10× than the helix refolding contribution. A closer look at the off-diagonal region reveals weak difference cross-peaks that connect the major features on the diagonal, e.g., I/III or II/IV.

Difference Cross-Peaks. The plot in Fig. 3 reveals a complex pattern of small cross-peaks, which reports on changes of vibrational couplings upon photoconversion. Another possible origin is a change in transition dipole strength, which would alter the magnitude of a cross-peak and would therefore also produce a difference signal. Contributions from different parts of the protein are marked in purple (BV), orange (β-sheet), and green (α-helix) and discussed as follows:
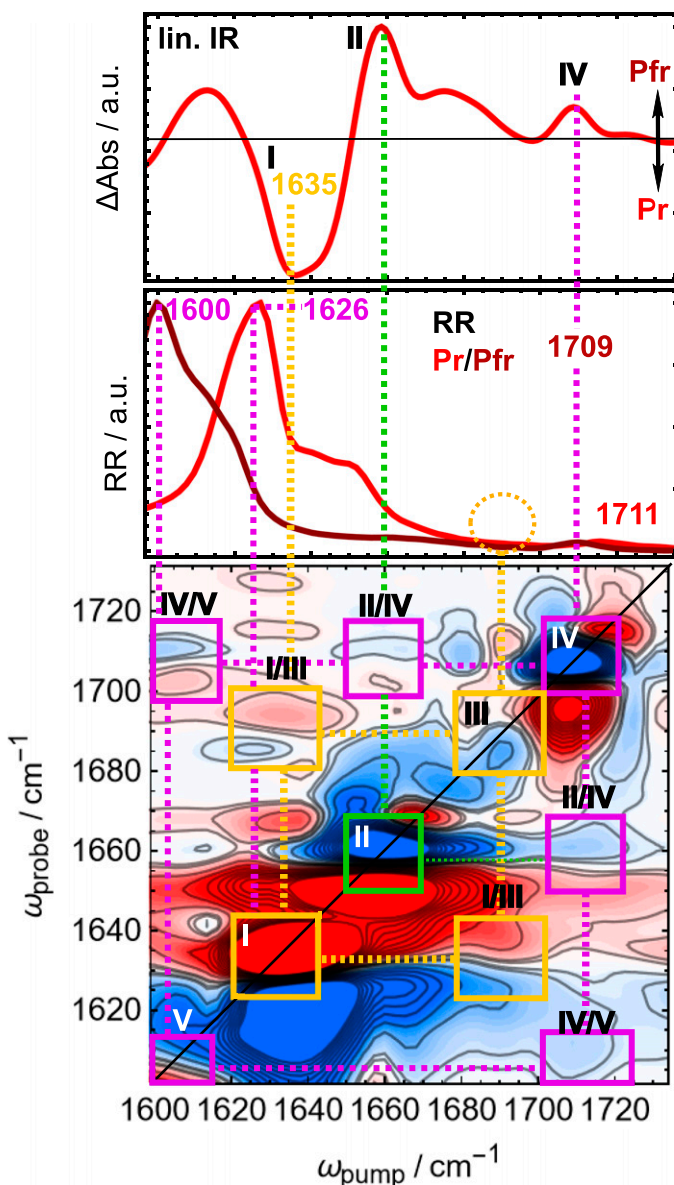

Fig. 3. (*Top*) Linear IR difference spectrum of Agp1. (*Middle*) RR spectra of Agp1 in the Pr and Pfr states. Data for *Middle* are taken from a previous publication (37). (*Bottom*) Pfr-minus-Pr difference 2D-IR spectrum. Roman numerals are discussed in detail in the main text, and signals originating from the β-hairpin are highlighted in orange, those from the α-helix in green, and those from BV modes in purple.

IV/V) A pair of positive cross-peaks that connects CO_D with a diagonal feature (V) outside the amide I region around 1,600 cm^{-1} is detected. This signal coincides precisely with the position of the dominant C = C stretching peak in the Pfr RR spectrum, indicating intramolecular vibrational coupling between the CO_D and C = C modes in Pfr. While this positive cross-peak is quite strong, a negative counterpart would be expected at 1,711/1,626 cm^{-1} due to Pr C = C and CO_D bleach at this frequency. Such a feature is barely visible, probably due to the broadened and therefore weaker CO_D band in Pr.

I/III) Cross-peaks with a negative sign are found at the position where the coupling between the β-sheet a– and a+ modes is expected and therefore assigned to the loss of β-sheet content due to tongue refolding. However, diagonal peak I also contains a contribution from the BV C = C stretching signal at 1,626 cm^{-1}, the strongest signal in the Pr RR spectrum. In contrast to peak I, cross-peak I/III likely does not contain contributions from the C = C stretching mode and solely originates from the β-sheet, because there are no BV modes around 1,690 cm^{-1} that could couple to the C = C and cause an off-diagonal feature at this position (dotted orange circle). Another option would be a highly localized protein mode at this position that couples with the C = C stretching only in Pr, which also appears unlikely.

II/IV) A positive cross-peak is observed between CO_D and the α-helix signal, indicating that CO_D couples stronger specifically to helix amide I modes in Pfr. In contrast to the broad feature in the absolute spectrum that extends over the entire amide I region, the difference cross-peak is quite sharp and localized at the α-helix position. While the increased dipole strength of CO_D increases the magnitude of the diagonal CO_D band and all related cross-peaks, the relative sharpness and localization of this peak at 1,660 cm^{-1} indicate that it truly originates from a coupling with an α-helical element in Pfr, in contrast to the broad cross-peaks in the absolute spectra in both states.

Discussion

Two-Dimensional Lineshapes and Cross-Peaks. The oscillator strength of the amide I modes of regular secondary structure motifs such as α-helices and β-sheets concentrates into a smaller number of normal modes, in which the C = O groups oscillate in phase, resulting in an increase in transition dipole strength by a factor of more than 2× (39). Together with the quadratic dependence of the 2D-IR signal, this results in narrower 2D-IR spectra compared to linear IR spectra for these secondary structure motifs. In Agp1, this narrowing of the amide I band significantly reduces the overlap with bands in adjacent regions and thus allows one to investigate the absolute CO_D lineshape in Pr and Pfr directly, which is not possible in linear IR experiments. Generally speaking, the amide I narrowing makes it possible to study all other vibrational modes with frequencies >1,700 cm^{-1} in this way. In photoreceptors, especially the C = O stretchings of protonated carboxylic sidechains that appear in bathy phytochromes (40), retinal proteins (41), cryptochromes (42), or photoactive yellow protein (43) are functionally relevant and therefore of high interest. The 2D-IR spectroscopy at low temperatures (44) or transient 2D-IR spectroscopy (45, 46) could potentially reveal dynamic changes in the lineshape as these photoreceptors progress

through their functional cycles. Here, these modes would act as local probes for the changing dynamics of their environment during the photocycle.

Furthermore, the 2D-IR difference technique spreads the congested linear spectra out into two dimensions, which is helpful for distinguishing between contributions of overlapping bands. For example, cross-peak I/III exclusively serves as a marker for the β-sheet loss, in contrast to diagonal feature I that overlaps with the C = C stretching vibration. Altogether, three systems of cross-peaks were observed in the difference 2D-IR spectrum that appear at consistent positions above and below the main diagonal. These three systems report on different types of coupling. Cross-peak IV/V originates from two localized and adjacent chromophore modes, which are very likely mechanically coupled to each other. Cross-peak I/III originates from two modes that are likely delocalized over the entire length of the tongue hairpin structure (47). Cross-peak II/IV is particularly interesting because here, a localized mode from the chromophore couples to a delocalized α-helix mode of the protein. Mechanical coupling through bonds appears unlikely because the CO_D group is ca. 20 bonds away from the closest amino acid, a cysteine residue that is covalently linked to BV pyrrole ring A (30, 48). Therefore, the most probable explanation for this cross-peak is an increased dipole coupling through space with the α-helical tongue region in the Pfr state.

Helix Stabilization in Pfr. The increased dipole coupling that leads to cross-peak II/IV can be rationalized by looking at the crystal structure of the Pfr-stabilized phytochrome Agp2, which we use as a model for the Pfr state in Agp1 (Fig. 4) (32). The strength of dipole coupling depends on the distance and angles between the individual dipoles, and CO_D is in close proximity
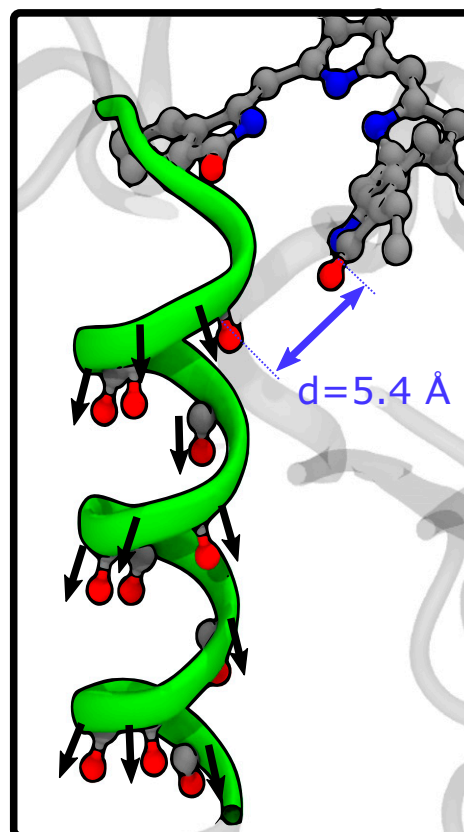

Fig. 4. Model for dipole stabilization of the *15E* configuration of BV and the helical structure of the tongue region in the Pfr state. The alignment of the C = O dipoles results in increased vibrational coupling.

to the tongue in Pfr. All peptide CO groups in α-helices point in one direction, and thus their individual dipoles add up and couple strongly between each other. In the case of Agp2, 11 peptide groups (amino acids PRO459 to THR469) contribute to the overall helix backbone dipole. The distance of CO_D to the closest CO group of that helix (PRO459) is only 5.4 Å in Pfr (Fig. 4), while ring D and the tongue region do not interact directly in Pr (compare Fig. 1).

Studies of a truncated Agp1 variant lacking the tongue region showed that Pfr is not stabilized properly (23, 49), as indicated by a strongly broadened vis absorption and accelerated dark reversion to Pr. Similar results were found for other bacterial phytochromes, indicating that this a general effect in canonical Bphs (37, 50). Therefore, we propose that the interaction between the tongue helix and CO_D we detect here in the form of a cross-peak might play a role in stabilizing the position of pyrrole ring D in Pfr and thus contributes to the kinetic stabilization of Pfr on timescales between minutes and days. The timescale of dark reversion is a highly variable parameter in different phytochromes and important for fine-tuning of the amount of active state in photostationairy equilibrium and therefore the biological function. Here, it is important to recall that it is the transition dipole coupling that gives rise to cross-peaks in a 2D-IR spectrum, while it is dipole interactions that may electrostatically stabilize a structure. The amide I mode is in essence the vibration of a diatomic molecule, i.e., the polar C = O group of the protein backbone, in which case the transition dipole is directly related to the dipole. The idea of dipole stabilization is further supported by the homogeneous 2D lineshape of CO_D in Pfr, which indicates a well-defined single structure in this state.

The other way around, one might also speculate that isomerization and repositioning of CO_D could act as a driving force for the refolding of the tongue into the helical configuration. It has for example been shown that coupling of an external electronic dipole to a peptide can function in this way and trigger the folding of a random coil into a helix (51). However, in this example, the electronic dipole was much larger than in CO_D. On the other hand, that study considered an isolated peptide that did not interact with the rest of a larger protein. We estimated the dipolar interaction energy between CO_D and the helix backbone carbonyls by extracting the coordinates of all relevant C = O groups from the Agp2 Pfr crystal structure (Fig. 4) and assuming charges of 0.5 e and –0.5 e for the C and O atoms,

respectively. This model calculation yielded a high interaction energy with the first C = O group of ca. 2 kJ/mol, while the 10th C = O group contributes only with an energy of 50 J/mol due to the strong distance dependence. The entire helix adds up to ca. 3.8 kJ/mol or 1.5 k_B T. It is clear that many strongly competing forces are responsible for the structure of a protein, and energies on this order of magnitude might have large net effects. Overall, we suggest that the observation of the dipolar interaction is related to the evident mutual stabilization of these two sites and the corresponding cross-peak might be used as a marker for the interaction between them in future studies.

Methods

Agp1 (PAS-GAF-PHY) samples were prepared according to published protocols in a Tris buffer containing 50 mM Tris-Cl, 5 mM EDTA, and 300 mM NaCl and adjusted with HCl and NaOH to pH 7.8 (48). The 2D-IR spectra were collected with a setup based on a 100-kHz Yb-fiber laser, mid-IR optical parametric amplifier (OPA), and a pulse shaper as described before in detail (35, 46). Here, the 2D-IR spectra were collected in the rotating frame with a reference frequency of 1,450 cm^{-1}, while the step size for scanning the t_1 delay was 40 fs, and the t_2 delay was 200 fs for all measurements. During data collection, the sample was illuminated inside the setup with two different light sources to photoswitch between the Pr and Pfr states. Here, a red LED (LIU630A; Thorlabs) was used to populate the Pfr state, while a far-red diode laser (L785P25) was used for Pr. The individual absolute spectra of each state were collected for 30 min, corresponding to an averaging of 10^6 individual 2D-IR spectra. This process for Pr and Pfr was repeated 10 times and the average of all data was used for analysis. UV-vis absorption spectra were recorded before and after the 2D-IR measurements, and no signs of photodegradation were found in these spectra or in 2D-IR spectra at different time points during the accumulation. All measurements were performed in aqueous (H_2O) buffer solution, and the pathlength of the sample cell was 5 μm. The concentration of the sample was 10 mM, determined by measuring the optical density at 280 nm in the same cell used for the 2D-IR measurements and using an extinction coefficient of ε_{280} = 78,505 mol^{-1} · cm^{-1} (from Protein Data Bank) to calculate the concentration.

1. K. Anders, L. O. Essen, The family of phytochrome-like photoreceptors: Diverse, complex and multi-colored, but very useful. *Curr. Opin. Struct. Biol.* **35**, 7–16 (2015).
2. W. L. Butler, K. H. Norris, H. W. Siegelman, S. B. Hendricks, Detection, assay, and preliminary purification of the pigment controlling photoresponsive development of plants. *Proc. Natl. Acad. Sci. U.S.A.* **45**, 1703–1708 (1959).
3. A. C. Froehlich, B. Noh, R. D. Vierstra, J. Loros, J. C. Dunlap, Genetic and molecular analysis of phytochromes from the filamentous fungus *Neurospora crassa. Eukaryot. Cell* **4**, 2140–2152 (2005).
4. T. Lamparter et al., Characterization of recombinant phytochrome from the cyanobacterium Synechocystis. *Proc. Natl. Acad. Sci. U.S.A.* **94**, 11792–11797 (1997).
5. Z. Jiang et al., Bacterial photoreceptor with similarity to photoactive yellow protein and plant phytochromes. *Science* **285**, 406–409 (1999).
6. S. H. Bhoo, S. J. Davis, J. Walker, B. Karniol, R. D. Vierstra, Bacteriophytochromes are photochromic histidine kinases using a biliverdin chromophore. *Nature* **414**, 776–779 (2001).
7. D. M. Shcherbakova, M. Baloban, V. V. Verkhusha, Near-infrared fluorescent proteins engineered from bacterial phytochromes. *Curr. Opin. Chem. Biol.* **27**, 52–63 (2015).
8. G. Gourinchas, S. Etzl, A. Winkler, Bacteriophytochromes - from informative model systems of phytochrome function to powerful tools in cell biology. *Curr. Opin. Struct. Biol.* **57**, 72–83 (2019).
9. B. Karniol, R. D. Vierstra, The pair of bacteriophytochromes from *Agrobacterium tumefaciens* are histidine kinases with opposing photobiological properties. *Proc. Natl. Acad. Sci. U.S.A.* **100**, 2807–2812 (2003).
10. E. Multamäki et al., Comparative analysis of two paradigm bacteriophytochromes reveals opposite functionalities in two-component signaling. *Nat. Commun.* **12**, 4394 (2021).
11. G. Gourinchas et al., Long-range allosteric signaling in red light-regulated diguanylyl cyclases. *Sci. Adv.* **3**, e1602498 (2017).
12. H. Takala et al., Signal amplification and transduction in phytochrome photosensors. *Nature* **509**, 245–248 (2014).
13. J. R. Wagner, J. S. Brunzelle, K. T. Forest, R. D. Vierstra, A light-sensing knot revealed by the structure of the chromophore-binding domain of phytochrome. *Nature* **438**, 325–331 (2005).
14. X. Yang, E. A. Stojković, J. Kuk, K. Moffat, Crystal structure of the chromophore binding domain of an unusual bacteriophytochrome, RpBphP3, reveals residues that modulate photoconversion. *Proc. Natl. Acad. Sci. U.S.A.* **104**, 12571–12576 (2007).
15. C. Song et al., Solid-state NMR spectroscopy to probe photoactivation in canonical phytochromes. *Photochem. Photobiol.* **89**, 259–273 (2013).
16. E. S. Burgie et al., Crystallographic and electron microscopic analyses of a bacterial phytochrome reveal local and global rearrangements during photoconversion. *J. Biol. Chem.* **289**, 24573–24587 (2014).
17. H. Takala et al., Light-induced structural changes in a monomeric bacteriophytochrome. *Struct. Dyn.* **3**, 054701 (2016).
18. G. Battocchio, R. González, A. G. Rao, I. Schapiro, M. A. Mroginski, Dynamic properties of the photosensory domain of *Deinococcus radiodurans* bacteriophytochrome. *J. Phys. Chem. B* **124**, 1740–1750 (2020).
19. J. A. Ihalainen et al., Chromophore-protein interplay during the phytochrome photocycle revealed by step-scan FTIR spectroscopy. *J. Am. Chem. Soc.* **140**, 12396–12404 (2018).
20. D. Buhrke, U. Kuhlmann, N. Michael, P. Hildebrandt, The photoconversion of phytochrome includes an unproductive shunt reaction pathway. *ChemPhysChem* **19**, 566–570 (2018).
21. J. Dasgupta, R. R. Frontiera, K. C. Taylor, J. C. Lagarias, R. A. Mathies, Ultrafast excited-state isomerization in phytochrome revealed by femtosecond stimulated Raman spectroscopy. *Proc. Natl. Acad. Sci. U.S.A.* **106**, 1784–1789 (2009).
22. J. J. van Thor, K. L. Ronayne, M. Towrie, Formation of the early photoproduct lumi-R of cyanobacterial phytochrome cph1 observed by ultrafast mid-infrared spectroscopy. *J. Am. Chem. Soc.* **129**, 126–132 (2007).
23. P. Piwowarski et al., Light-induced activation of bacterial phytochrome Agp1 monitored by static and time-resolved FTIR spectroscopy. *ChemPhysChem* **11**, 1207–1214 (2010).

24. H. Foerstendorf *et al.*, FTIR studies of phytochrome photoreactions reveal the C=O bands of the chromophore: Consequences for its protonation states, conformation, and protein interaction. *Biochemistry* **40**, 14952–14959 (2001).

25. E. A. Stojković *et al.*, FTIR spectroscopy revealing light-dependent refolding of the conserved tongue region of bacteriophytochrome. *J. Phys. Chem. Lett.* **5**, 2512–2515 (2014).

26. A. Kraskov *et al.*, Intramolecular proton transfer controls protein structural changes in phytochrome. *Biochemistry* **59**, 1023–1037 (2020).

27. Z. Ganim *et al.*, Amide I two-dimensional infrared spectroscopy of proteins. *Acc. Chem. Res.* **41**, 432–441 (2008).

28. P. Hamm, M. T. Zanni, *Concepts and Methods of 2D Infared Spectroscopy* (Cambridge University Press, 2011).

29. T. Lamparter, N. Krauss, P. Scheerer, Phytochromes from *Agrobacterium fabrum*. *Photochem. Photobiol.* **93**, 642–655 (2017).

30. S. Nagano *et al.*, The crystal structures of the N-terminal photosensory core module of *Agrobacterium* phytochrome Agp1 as parallel and anti-parallel dimers. *J. Biol. Chem.* **291**, 20674–20691 (2016).

31. A. Takiden *et al.*, Structural and vibrational characterization of the chromophore binding site of bacterial phytochrome Agp1. *Photochem. Photobiol.* **93**, 713–723 (2017).

32. A. Schmidt *et al.*, Structural snapshot of a bacterial phytochrome in its functional intermediate state. *Nat. Commun.* **9**, 4912 (2018).

33. N. Demirdöven *et al.*, Two-dimensional infrared spectroscopy of antiparallel beta-sheet secondary structure. *J. Am. Chem. Soc.* **126**, 7981–7990 (2004).

34. L. Chuntonov, R. Kumar, D. G. Kuroda, Non-linear infrared spectroscopy of the water bending mode: Direct experimental evidence of hydration shell reorganization? *Phys. Chem. Chem. Phys.* **16**, 13172–13181 (2014).

35. J. Ruf, P. Hamm, D. Buhrke, Needles in a haystack: H-bonding in an optogenetic protein observed with isotope labeling and 2D-IR spectroscopy. *Phys. Chem. Chem. Phys.* **23**, 10267–10273 (2021).

36. C. Schumann, R. Gross, N. Michael, T. Lamparter, R. Diller, Sub-picosecond mid-infrared spectroscopy of phytochrome Agp1 from *Agrobacterium tumefaciens*. *ChemPhysChem* **8**, 1657–1663 (2007).

37. D. Buhrke *et al.*, Distinct chromophore-protein environments enable asymmetric activation of a bacteriophytochrome-activated diguanylate cyclase. *J. Biol. Chem.* **295**, 539–551 (2020).

38. G. Merga *et al.*, Light- and temperature-dependent dynamics of chromophore and protein structural changes in bathy phytochrome Agp2. *Phys. Chem. Chem. Phys.* **23**, 18197–18205 (2021).

39. M. Grechko, M. T. Zanni, Quantification of transition dipole strengths using 1D and 2D spectroscopy for the identification of molecular structures via exciton delocalization: Application to α-helices. *J. Chem. Phys.* **137**, 184202 (2012).

40. F. Velázquez Escobar *et al.*, A protonation-coupled feedback mechanism controls the signalling process in bathy phytochromes. *Nat. Chem.* **7**, 423–430 (2015).

41. K. Gerwert, G. Souvignier, B. Hess, Simultaneous monitoring of light-induced changes in protein side-group protonation, chromophore isomerization, and backbone motion of bacteriorhodopsin by time-resolved Fourier-transform infrared spectroscopy. *Proc. Natl. Acad. Sci. U.S.A.* **87**, 9774–9778 (1990).

42. T. Kottke, V. A. Lórenz-Fonfría, J. Heberle, The grateful infrared: Sequential protein structural changes resolved by infrared difference spectroscopy. *J. Phys. Chem. B* **121**, 335–350 (2017).

43. Y. Imamoto *et al.*, Low-temperature Fourier transform infrared spectroscopy of photoactive yellow protein. *Biochemistry* **40**, 8997–9004 (2001).

44. A. Shalit, F. Perakis, P. Hamm, Communication: Disorder-suppressed vibrational relaxation in vapor-deposited high-density amorphous ice. *J. Chem. Phys.* **140**, 151102 (2014).

45. H. S. Chung, Z. Ganim, K. C. Jones, A. Tokmakoff, Transient 2D IR spectroscopy of ubiquitin unfolding dynamics. *Proc. Natl. Acad. Sci. U.S.A.* **104**, 14237–14242 (2007).

46. P. Hamm, Transient 2D IR spectroscopy from micro- to milliseconds. *J. Chem. Phys.* **154**, 104201 (2021).

47. A. W. Smith, H. S. Chung, Z. Ganim, A. Tokmakoff, Residual native structure in a thermally denatured beta-hairpin. *J. Phys. Chem. B* **109**, 17025–17027 (2005).

48. T. Lamparter *et al.*, Biliverdin binds covalently to agrobacterium phytochrome Agp1 via its ring A vinyl side chain. *J. Biol. Chem.* **278**, 33786–33792 (2003).

49. S. Noack, N. Michael, R. Rosen, T. Lamparter, Protein conformational changes of *Agrobacterium* phytochrome Agp1 during chromophore assembly and photoconversion. *Biochemistry* **46**, 4164–4176 (2007).

50. J. R. Wagner *et al.*, Mutational analysis of *Deinococcus radiodurans* bacteriophytochrome reveals key amino acids necessary for the photochromicity and proton exchange cycle of phytochromes. *J. Biol. Chem.* **283**, 12212–12226 (2008).

51. C. Y. Huang, S. He, W. F. DeGrado, D. G. McCafferty, F. Gai, Light-induced helix formation. *J. Am. Chem. Soc.* **124**, 12674–12675 (2002).

52. D. Buhrke, Data for "Vibrational couplings between protein and cofactor in bacterial phytochrome Agp1 revealed by 2D-IR spectroscopy." Zenodo. https://zenodo.org/record/6757659. Deposited 27 June 2022.